A Nonlinear System Science Approach to Find the Robust Solar Wind Drivers of the Multivariate Magnetosphere

S. Blunier[1], B. Toledo[1,2], J. Rogan[1,2], J. A. Valdivia[1,2]

[1]Departamento de Física, Facultad de Ciencias, Universidad de Chile, Santiago, Chile
[2]Centro para el Desarrollo de la Nanociencia y Nanotecnologia, CEDENNA, Santiago, Chile

Abstract

We propose a method, based on Neural Networks, that detects the nonlinear robust interplanetary solar wind variables, with varying delays, driving the coupled behavior of three geomagnetic indices (Dst, AL, and AU). As opposed to minimizing a prediction error, the method is based on degrading the prediction by distorting the inputs of the trained Neural Networks in order to highlight the most sensible drivers. We show that the z component of the magnetic field, the duskward oriented electric field, and the speed of the particles of the interplanetary medium, at particular time delays, seem to be the most efficient drivers of the three coupled geomagnetic indices. Using only the sensible or robust drivers in the model, we demonstrate that iterated predictions during geomagnetic storm are significantly improved from models that only use one of the outstanding drivers with multiple time delays. The derived robust nonlinear Neural Network model is also a significant improvement over linear approximations, specially when used as iterated predictors.

1 Introduction

The study of the solar wind-magnetosphere-ionosphere (SWMI) coupled system has become a relevant subject of wide interest, not only because of its scientific repercussions, but also for its application in space weather forecasts (e.g. Hapgood (2018); Camporeale (2019); Bala and Reiff (2018)). As such, constructing models that are able to describe certain characterizations of the SWMI system in a robust manner can have important social and economical consequences for our countries, and the world in general, since space weather can affect a number of human activities such as mining, natural disaster management, remote communications, precise farming, aircraft traffic communication, power grid management, etc (e.g. Hapgood (2018); Council (2008)).

It is well known that the Sun activity can affect the Earth magnetosphere and ionosphere (Gosling, 2000). This can be quickly realized by observing the simultaneous evolution of a number of solar wind parameters and magnetospheric indices that are used to monitor the magnetospheric and ionospheric activity. For example the Disturbance Storm-Time (Dst) index is used to describe the horizontal magnetic field variations close to the magnetic equator. Hourly Dst indices since 1957 have been derived by Sugiura (1964), and more recently, they are available, in real-time, at the World Data Center in Kyoto in Japan. The Dst is likely the most studied index in relation to geomagnetic storms, for example, Burton et al. (1975) constructed a linear evolution model driven by the solar wind VBs and dynamic pressure P. Here V is the bulk ion velocity, B_s is the southward component of the interplanetary magnetic field. Further studies and discussions suggested that the Dst evolution may be nonlinear (J. A. Valdivia et al., 1996; Vassiliadis et al., 1999) and that more magnetospheric and solarwind variables should be considered to represent storm time space-weather phenomena (Borovsky & Shprits, 2017; Borovsky, 2020).

Similarly, the upper AU and lower AL auroral indices, representing the envelopes of the magnetic fields variations taken from around 12 high latitude geomagnetic observatories (Davis & Sugiura, 1966), provide complementary information about a different region of the SWMI system. There has been a number of studies that strongly suggest that the solar wind driven dynamics of AL and AU are nonlinear (Bargatze et al., 1985; Vassiliadis et al., 1995, 2000).

Furthermore, a system science approach very quickly reveals that there are complex interactions among the different regions of the magnetosphere and the solar wind (Borovsky & Valdivia, 2018). Hence, the inherent complexity of the SWMI system (J. A. Valdivia et al., 2005; J. Valdivia et al., 2013; Consolini et al., 2018; Donner et al., 2019), demands the development of models and techniques to account for these interactions in a robust manner.

This is becoming particularly true as we are increasingly relying on artificial intelligence models to try to account for such complex behavior (Bortnik et al., 2018; Jawad et al., 2019). However, when developing robust models, it is not enough to just train a neural net with a large number of variables since, given the complex and nonlinear nature of the system, the model will probably not work as efficient on a set of events that is different from the training set. Therefore, we need to identify what are the robust variables, among all accessible ones, that should be included when constructing a simplified representation of the SWMI system such that it still works on a different set of events.

Hence, a robust multivariate nonlinear system science description, that for example includes the coupling of these 3 magnetospheric indices (MI) and with solar wind drivers (Borovsky & Denton, 2018; J. A. Valdivia et al., 1999) can further our understanding of these interactions and their time scales (Adhikari et al., 2020), and could pave the way to robust Space Weather applications. This is what we are going to start analyzing in this manuscript. So that, for simplicity, we will study the 3 above described geomagnetic or magnetospheric indices (MI) ($Dst(t)$,$AL(t)$ and $AU(t)$) and search for the robust solar wind variables (SWV), and their possible time delays, that drive the magnetosphere response as characterized by these 3 indices. In our study we will consider data with an hour time scale and let faster variation to future work.

As a model reconstruction, we will use Neural Networks (NN) because they have demonstrated to be a powerful machine learning tool capable of performing complex tasks (Abiodun et al., 2018). NN have already been used to forecast the Dst index (Lazzus et al., 2017; Gruet et al., 2018) showing that it has a high self correlation with the immediate past measurements, therefore, the NN will include the Dst index at time t as part of the NN variables. The same will be done for the other magnetospheric indices that we are considering here.

A huge advantage of NN is their capability to build functions that can be highly non-linear and that property is the one we want to exploit in the present study. The counterpart is that once they are trained, they are a black box which parameters remain meaningless to humans. We are therefore strongly limited to extract valuable physical information from what they could have "learned". Furthermore, it is very common that their predictability could be quite high in the training set, but not as good in out-of-sample forecasting of other events. In the present manuscript we purpose a method that quantifies the robustness of a solar wind variable as the degradation of the predictability of the trained model when such a variable is perturbed trying to forecast a different testing set of events. The most sensitive or robust variables, are those which produce the largest error when perturbed over the testing set.

In the present study we address the model construction in two ways. First we consider a short term prediction that uses the selected solar wind variables, and their delays, at a particular moment in order to predict the geomagnetic indices for the next hour, which we call *one step forecasting*. The second way is to use the one step prediction model to forecast the MI for a longer time interval, using the selected SWV, and their time delays, and reinserting the predicted geomagnetic indices in the model, which we will call *iterated forecasting*.

In order to simulate real-time forecasting we use the *iterated forecasting*, since we note that some of these indices are not easily accessible in real time or are available only part of the time.

If successful, our approach would provide a strong indication that the selected robust inputs drive the signal and brings information about the physics of the system. This information could be used as a complementary approach to test, validate, and optimize forecasting models of the magnetospheric response to solar wind input, and in general of any driven complex system under study. For example, predictions of the Dst index

are provided by many services like the Space Weather Center Prediction, or `www.spaceweatherlive.com`. Their short term accuracy could be tested, improved, and optimize by following our strategy to find robust modes of interaction. Additionally, since our strategy of constructing these forecasting models is quite different from the standard ones, it is always useful to provide an alternative forecast, specially during periods where real-time *Dst* may not be available. The same can be said about AL and AU, which are usually not easily available in real time.

2 Data description

The values of the *Dst* index are provided hourly from year 1957 to the present at the World Data Center for Geomagnetism in Kyoto, they can be found at `http://wdc.kugi.kyoto-u.ac.jp/dstdir/index.html` ((Masahito et al., 2015)). No value is missing since 1957, thus no signal reconstruction is needed. We will then use the hourly resolution in all the study Data of interplanetary medium and the AU and AL indices where retrieved from the OMNI database provided by the National Aeoronautic and Spatial Agency and freely available at `ftp://spdf.gsfc.nasa.gov/pub/data/omni/high_res_omni/` ((King & Papitashvili, 2005)). The oldest available data in OMNI is from 1963 but with an average data rate lower than 20% which is too sporadic for our purposes. From year 1995 the data rate improved significantly thanks to the Wind and ACE satellites commissioning.

OMNI data are provided with a resolution of one minute but are not continuous. Since *Dst* is provided hourly, we choose to perform this study using a resolution of one hour, therefore OMNI data need to be transformed to one hour sampling.Values are taken when the UTC minute is equal to 0 and will be calculated as the average over all available data of the 60 following minutes. Even if only one value is available during this hour it will be taken as the value of the corresponding hour. In case no data is provided during this interval, they will be generated with by a linear interpolation from the available values.

The SWV that we use from the OMNI database are the three interplanetary magnetic field (IMF) components given in the GSE coordinate system (B_x, B_y, B_z), the particle flow speed (V), the proton number density (N), the plasma temperature (T), and the proton dynamical pressure (p). It is worth noticing that p is not a direct measurement but it is calculated from the proton speed and density by $p = 2{\times}10^{-6}NV^2$(nPa). We can also construct composed variables that will be considered in the analysis. One is VB_s, where B_s is the negative component of Bz, so that it is zero if $B_z > 0$ and B_z if $B_z < 0$. Sometimes, people prefer to write this expression in the GSM coordinate system, but for our purpose we stay within the GSE coordinate system just to demonstrate that we can include composed indexes in the analysis. Similarly, we define $\varepsilon_A = VB^2 \sin^4(\theta/2) l_0^2$, where B as the magnitude of the IMF, l_0 is seven times the Earth radii, and the clock angle θ is $\tan^{-1}(|B_y/B_z|)$ for $B_z > 0$ and $\pi - \tan^{-1}(|B_y/B_z|)$ for $B_z < 0$. When using variables in the GSM coordinate system, such formula would describe the Akasofu's index.

All the used interplanetary variable are summarized in Table 1 with their units and typical values in quiet and disturbed times, they will all be treated as independent variables.

Since we are interested in studying perturbations of the magnetosphere, we will concentrate on geomagnetic storms intervals where the *Dst* index reach a climax below $-100\,\mathrm{nT}$. We consider the storm is over the first time that *Dst* reach $Dst_{end} > -10\,\mathrm{nT}$ after the climax. The beginning of the storm is taken T_b hours before the climax, such that T_b is 20% of the time that separates the climax to the end of the storm. Between 1995 and 2018 we identify 97 geomagnetic storms that reach a climax below $-100\,\mathrm{nT}$. In order

SW signal	Symbol	Quiet	Storm	Unit
3 Magnetic field components	$B_{x,y,z}$	$\lvert B_{x,y,z}\rvert \leq 10$	$\lvert B_{x,y,z}\rvert > 10$	nT
Flow speed	V	$300 - 400$	> 500	$\mathrm{km\,s^{-1}}$
VB_s parameter	VB_s	0	< -4000	$\mu\mathrm{V\,s^{-1}}$
Pressure	P	$0 - 5$	> 5	nPa
Temperature	T	$10^4 - 10^5$	$> 2 \times 10^5$	K
Number density	N	$1 - 10$	> 15	# particles/cc
ϵ_A parameter	ϵ_A	$< 10^{11}$	$> 10^{11}$	Watt

Table 1. Solar wind variables that are analyzed for their capability to drive the geomagnetic indices considered here. We give their mathematical symbol, their typical values during quiet and active periods, and their units. To be used for the neural net analysis, all variables will be mapped to the range between $[0, 1]$, so their absolute values and units will not be extremely relevant in the rest of the development.

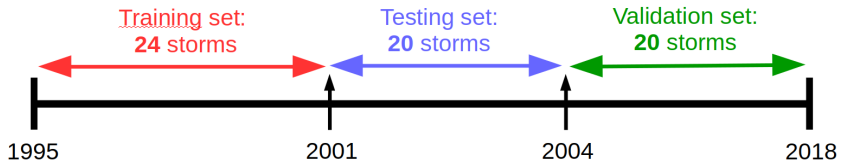

Figure 1. Separation of storms for training, testing, and validation sets, the first 24 storms will be used for training, the following 20 storms for the testing phase, and the last 20 storms for the validation step.

to improve the robustness of the data we require that all the variables used during the time of the storm fulfill with the following criteria: (a) a maximum of 5 continuous hours with no data, and (b) at least 90% of data available during the storm interval. After applying those filters we have a set of 64 storms between 1995 and 2018 that will be used for our study.

3 Analysis

The 64 selected storms are split in training, testing, and validation sets as described in figure 1. In order to train and test our NN we use the Keras library under python. All data are scaled with the *MinMaxScaler* from the python *sklearn* library.

For the training phase we use the default Keras binary cross entropy loss function defined as:

$$C = -\frac{1}{N}\sum_{j=1}^{N_{out}} \left[y_j \ln \bar{y}_j^L + (1 - y_j) \ln(1 - \bar{y}_j^L) \right],$$

where N_{out} corresponds to the number of outputs of the NN, y_j are the normalized data values, $\hat{y}_j$ are the normalized output predicted by the NN. This function is non-negative and converge to zero when $\hat{y}_j$ gets closer to y_j. The minimization if performed with the Keras *adam* optimizer.

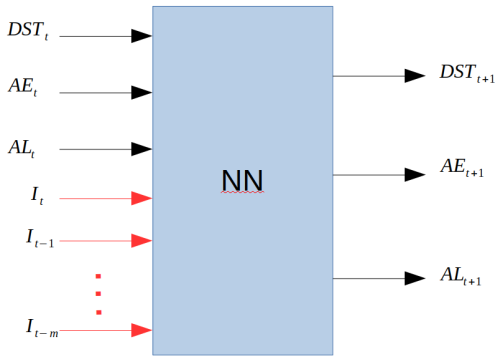

Figure 2. Input/Output variables used to train and test the NN in the case of a single solar wind driver ($n = 1$). The general case with multiple solar wind drivers follows the same pattern. Note that the magnetospheric variables in the evolution model are considered, for simplicity, only at the previous time t. This will be generalized in a future work.

All our NN have 3 hidden layers of 100 neurons activated with a sigmoid function. This allows us to describe a reasonably complex evolution function, given by

$$\bar{\mathbf{G}}_{t+1} = NN(\mathbf{G}_t, \mathbf{I}_t), \tag{1}$$

which gives us the value of the GI at $t+1$ from information at previous times. From now on, the bar on top of a variable means it is generated by the NN model. Here $\mathbf{G}_t$ corresponds to the magnetospheric vector

$$\mathbf{G}_t = (Dst_t, AU_t, AL_t),$$

while $\mathbf{I}_t$ corresponds to a set of solar wind drivers, possibly at different time delays, namely

$$\mathbf{I}_t = (I_{1,t-1}, \cdots, I_{1,t-m_i}, \cdots, I_{n,t-1}, \cdots, I_{n,t-m_n}),$$

where $I_{n,t}$ is the n^{th} solar wind driver at time t. The 9 solar wind drivers are described in table 1 and we will study their capability to robustly drive $\mathbf{G}_t$. In our study we will take, at most, $m_i = m = 10$ for all solar wind drivers, so that we will be able to check the influence of each solar wind driver on the magnetospheric variables up to 10 hours in the past. The NN is trained to make one step forecasting using the evolution function given by Eq. 1. The global structure of the NN for the training and testing phases is represented in Fig. 2.

In order to avoid over-fitting, at each epoch of the training phase, the cross entropy function is calculated using data from the testing set and is compared with the last best result obtained during the minimization. At each step, if the NN is better than the last best NN, it replaces it. This minimization process runs over 400 epochs, thus the NN corresponding to the last best epoch will be saved.

One of the difficulties of training NNs with real data is the multiple solution that can be found by the algorithm. The minimizing process can stabilize around a bad local minimum and then will miss the optimal solution. The best model of geomagnetic behavior prediction should be the NN that provides the lowest errors, even if we cannot guarantee that the algorithm has actually found the best solution. For each SWV of Table 1, we train around 40 NN and keep the best one for the testing phase.

In order to evaluate our models, we compare it to the toy model $\bar{\mathbf{G}}^p_{t+1} = \mathbf{G}_t$ that we call persistence model. For the testing and validation phases we compute the unitless mean absolute error (MAE) of a particular geomagnetic index X_t, normalized by the

error calculated in the persistence model, namely,

$$\epsilon_{MAE} = \frac{\sum_{t_i=1}^{t_f} \left| \bar{X}_{t+1} - X_{t+1} \right|}{\sum_{t_i=1}^{t_f} \left| \bar{X}^{p}_{t+1} - X_{t+1} \right|}. \tag{2}$$

The advantage of this measure is that it provides a direct comparison with the persistence model, but it also gives equal relevance to all the magnetospheric indices when we add the MAE for the 3 of them.

In order to evaluate the contribution of a particular solar wind driver, with a particular time delay, we will add to it a Gaussian noise centered in 0 and with an increasing standard deviation σ, such that the particular solar wind driver is now given by $I_{i,t-j} \rightarrow I_{i,t-j} + \delta_t^{(i,j)}$. All the other solar wind drivers are not perturbed. Here, σ will vary from 0% to 100% of the difference between the maximum and the minimum values obtained in the particular solar driver signal during the tested storm interval. If the NN is well trained, the noised introduced to the particular solar wind driver, at the particular time delay, is expected to degrade the prediction; and the higher the value of σ, the higher should be the ϵ_{MAE}. This will be called the noised input method. This analysis is then repeated on the same NN but perturbing another solar wind driver and/or time delay. We expect that the most robust solar wind drivers, at a particular time delay, are the ones that are most sensitive to the perturbation giving the largest error. Here we report the normalized MAE as $\epsilon(\sigma)/\epsilon(0) - 1$ for each of the geomagnetic indices.

To start, we train a NN that contains the geomagnetic indices and only one solar wind driver $I_{i,t}$ over the training set. We then perturb the same solar wind driver over the testing set, and observe its sensitivity with σ. We repeat the procedure for the other solar wind drivers, as shown in Fig. 3a-c for the storm of March 2001 that reached a pick value of $-149\,\mathrm{nT}$ for the Dst index.

For each trained NN that corresponds to a particular solar wind driver, the testing phase is repeated 50 times for each σ and we keep the average of the obtained error. Since the error is centered, all the curves begin at 0 for $\sigma = 0$. The solar wind driver is associated with one error per geomagnetic index. With this procedure, we expect to gain information on the correlation of the disturbed solar wind driver and its capability to predict $\mathbf{G}_t$.

We note that B_z and VB_s are consistently the most sensitive variables for the prediction of these 3 geomagnetic indices, which we will denote them the robust solar wind variables. For example, when the perturbations is of the size of the signal for Dst, meaning with $\sigma = 1$ the error is multiplied by 9 in the case of B_z and above 6 for VB_s, while the other drivers show a much lower perturbation when the noise increases. For the AL index, the effect is lower but still present, and B_z and VB_s remain by far the most sensitive solar wind drivers. Although in the case of AU the error does not reach more than 100% from the clean input for any of the solar wind drivers, still B_z and VB_s show up as relevant. Of course, for AU other variables could also be relevant such as density. Hence, we obtain an error for each geomagnetic index given a value of σ that informs us about the global robustness of the solar wind driver in the NN, and therefore, about the global robustness of this solar wind driver to predict $\mathbf{G}_t$. Let us note that the strategy we are using to determine the robust solar wind variables may at first sight seem counter intuitive, since we are not trying to minimize an error, but to maximize it. But after subsequent consideration, we hope it becomes more clear.

In order to provide a more general conclusion we repeat the experiment 50 times with $\sigma(\%) = 1$ for each storm. We show the average error over all the storms for each geomagnetic index and solar wind driver in Fig. 4. For a given magnetospheric index and solar wind driver we have a bin that represents how perturbed is the error when the input is noised, therefore, telling us about its contribution to the forecast. We also give

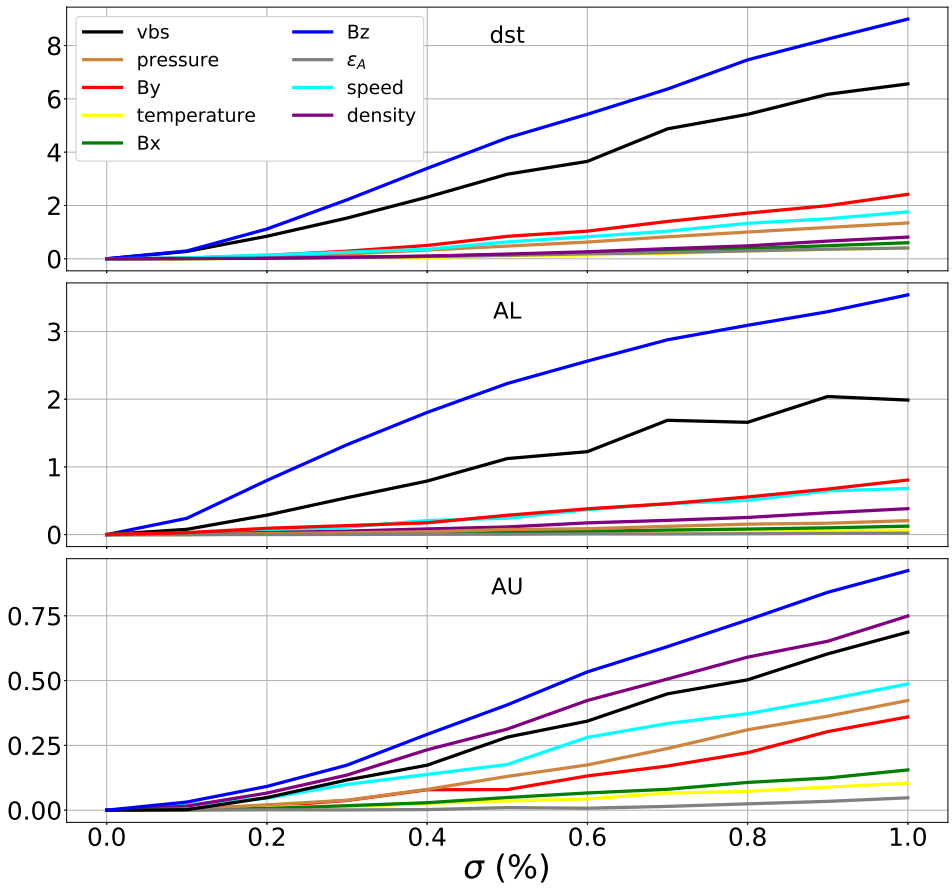

Figure 3. Evolution of the normalized MAE for each of the geomagnetic indices (a) Dst, (b) AL, and (c) AU with the amplitude of the noise σ during the storm of March 2001. The B_z and VB_s signals are consistently the most sensitive solar wind variables to the variation of σ while the others are not giving any strong evidence of contribution to the prediction.

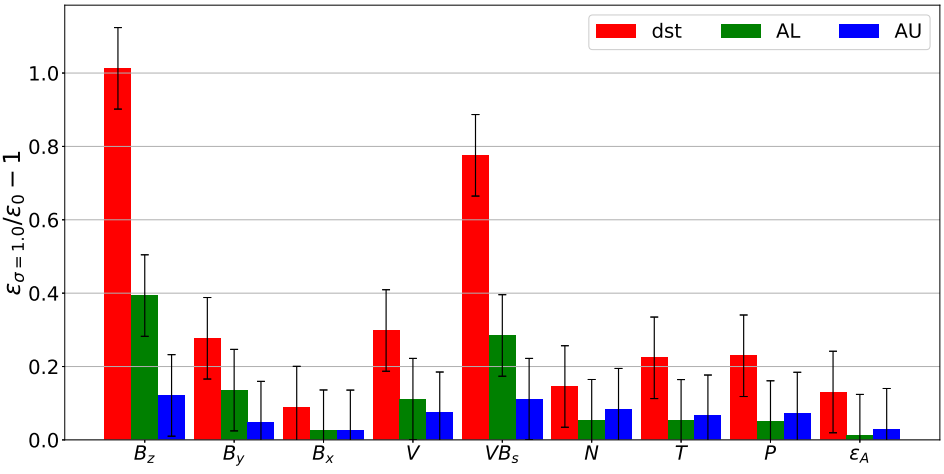

Figure 4. Summary of the response of each trained NN to the perturbed solar wind driver over all the storms in the testing set. The standard deviation of the error is also shown. We use 50 surrogates for each storm and solar wind driver. The most sensitive parameters are clearly B_z and VB_s.

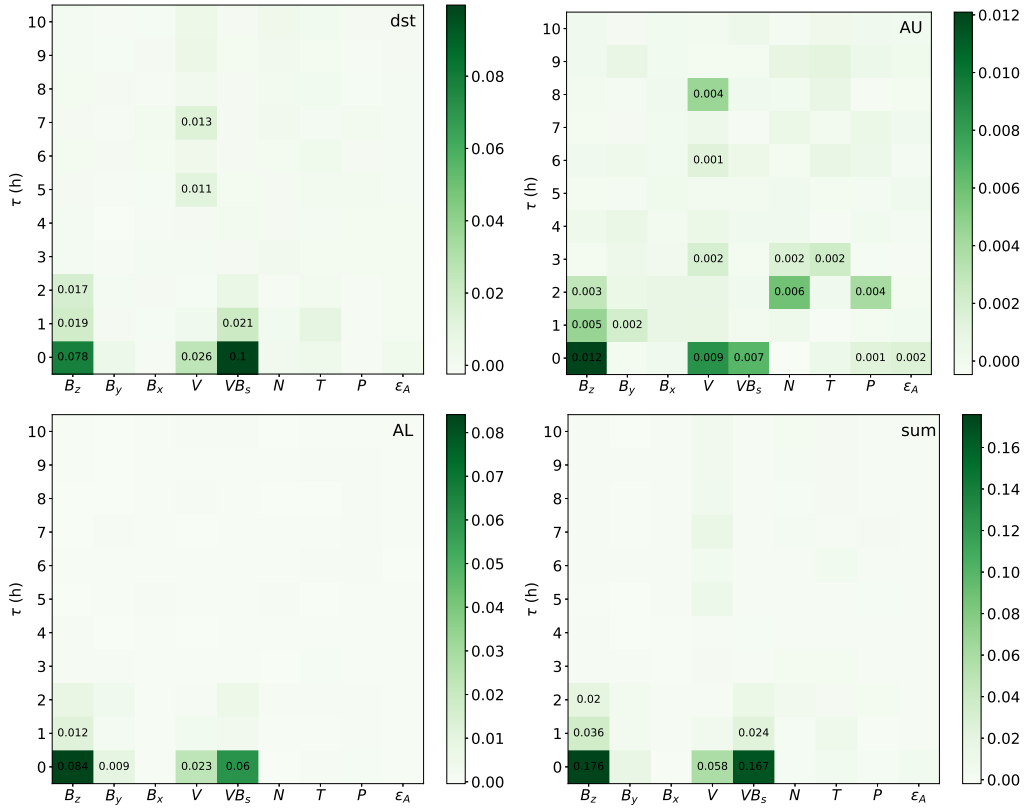

Figure 5. Summary of the response of the trained NNs to the randomization for each solar wind driver at each time delay τ considered in the entry. We show the error on (a) Dst, (b) AL, (c) AU, and (d) Sum of the previous 3. We note that only a few variables are relevant.

an error range that shows how stable is the perturbation. If the bar is compatible with 0, we can conclude that the driver is globally not contributing to the prediction. A global overview shows that the Dst index is the most sensitive to the solar wind drivers since the error is clearly higher than AU or AL. AU is not convincing in its sensitivity to the solar wind drivers, only B_z has a result not compatible with 0. From the point of view of the solar wind variables, we see again that B_z and VB_s are picked up by strategy as the most relevant solar wind variables to forecast the geomagnetic indices. The B_x and ϵ_A variables do not bring significant information to the prediction while the error produced by B_y, V, N, T, and P is quite reduced compared with the first two variables B_z and VB_s.

From now on, instead of adding an error to the signal we randomize the order of the solar wind driver time series for a particular storm (a surrogate). Using this randomization input method, we can look deeper inside the solar wind drivers. We are not only interested in identifying the solar wind variable that could contribute to predict the geomagnetic indices, but also at which time $t-\tau$ they should be taken to make a robust prediction. In order to find the most relevant components $I_{i,t-\tau}$ that affect the GI, we test the selected NN for each SWV at a particular time delay and repeat the surrogate randomizing procedure outlined above. Again, we expect that the most relevant components are the ones that should degrade the prediction the most. This procedure will produce one global associated error for each solar wind driver, at each time delay, of each geomagnetic index and each storm. Hence, it will give us clues about which solar wind drivers and delays should be used to construct a robust NN prediction model.

In Fig. 5a-c, we show the variation of the MAE produced by each component of each solar wind driver up to 10 hrs before the last available measurement for each geomagnetic index. We note that only a few solar wind variables, at particular time delays, are robust variables. Figure 5d displays the sum of the MAE for the 3 geomagnetic indices, providing a global descriptor of the robust solar wind drivers for this coupled system. We consider that a component contributes to the prediction (i.e., is robust) when it reaches 10% of the maximum value obtained in the matrix. For Dst, B_z is contributing up to 3 hours before the last measurement while VB_s only 2 hours. Some delayed components of the speed signal also seem to bring a significant contribution to the prediction. For AU, it looks that many components are turned on given the very low maximum, however, we can highlight the most important components being the immediate measurements of B_z, V, and VB_s. Finally AL has five components turned on, where again the last value of B_z and VB_s seem to be the best contributors. The global sum of the errors, shown in Fig. 5d, highlight 6 values which will be considered for our final robust model, namely, the 3 previous values of B_z, the last value of V, and the two last values of VB_s.

Once we have determined which are the most relevant solar wind drivers, at particular time delays, that drive the coupled geomagnetic indices, we train a robust NN replacing $\mathbf{I}_t$ by a vector containing those 6 components. Hence, we now retrain our NN with the global entry containing the same geomagnetic indices but with the 6 outstanding solar wind inputs of Fig. 5d. In parallel we build a linear model using the same entries for comparison.

As a matter of testing, we also want to use iterated predictions for the NN and linear model, meaning that they have to use the geomagnetic values they predicted $\bar{\mathbf{G}}_t$ in the previous time step to produce the next predicted value, namely,

$$\bar{\mathbf{G}}_{t+1} = NN(\bar{\mathbf{G}}_{t+1}, \tilde{\mathbf{I}}_t),$$

where $\tilde{\mathbf{I}}_t$ corresponds to the subset of 6 robust variables that are used as drivers of the neural net. Such approach may be useful for real time forecasts when only solar wind variables are available. One would naturally expect that the iterated predictions are less accurate than the one step predictions, that uses previously measured $\mathbf{G}_t$ values to drive the neural net. However it becomes relevant to compare these results with an equivalent model that does not consider the robustness of the variables. Therefore, as a way to compare, we construct NN and linear models using the 11 last measurements of the best driver B_z (left column of Fig. 5d). In Fig. 6a we plot the results over the validation set for the globally robust NN, while in Fig. 6b we show the results of the NN and linear models that use only the B_z driver at all time delays (11 inputs to the neural net). Each bin represents the normalized-by-persistence error for each geomagnetic index with a deviation bar for the 20 storms of the validation set.

In the case of one step forecasting of the robust model, although existent, the improvement do not look significantly different for both linear and NN models, but when we do iterated predictions the results becomes much more interesting. The prediction of Dst by the globally robust NN model are 38% (14.3% for AL, and 17.0% for AU) better than the linear model.

When comparing both robust and B_z-based nonlinear NN models, we find that for Dst and AU the iterated globally robust forecast show a global improvement of 12.7% and 8.7%, respectively, as compared with the B_z-based model. In the case of AL we obtain no improvement. Note that we have used 6 solar wind entries for the robust model, compared with the 11 solar wind entries of the B_z-based model. If we reduce the B_z-based model to only just the first 6 time delays, the difference is more notorious with respect to the robust model.

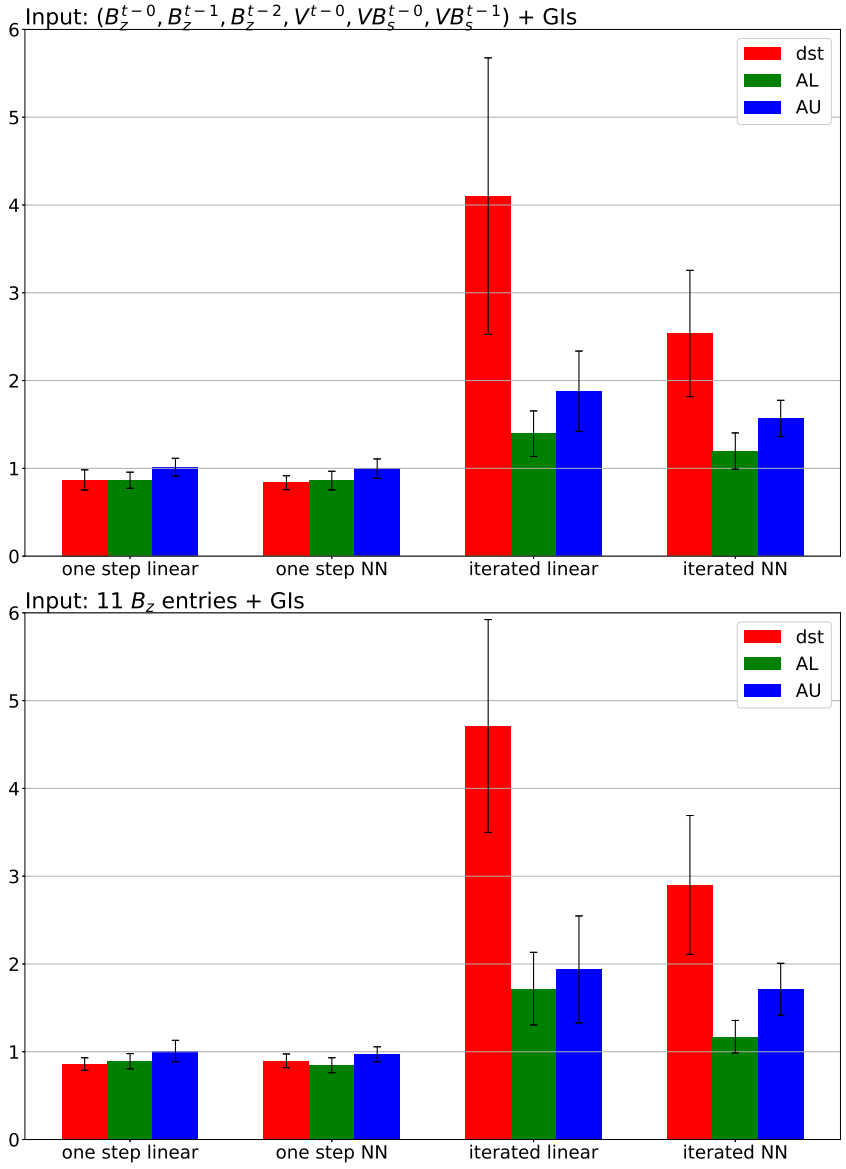

Figure 6. Normalized MAE for the (a) globally robust model, and (b) the model using the 11 last hours of B_z. We compare the NN versus a linear model using the same entries for one step and iterated predictions. The results are normalized with the error of the persistence. hence, the iterated forecasts using the nonlinear global robust model is an improvement from the equivalent model that uses only B_z variables, despite the fact that the later have a larger number of inputs (11 vs 6).

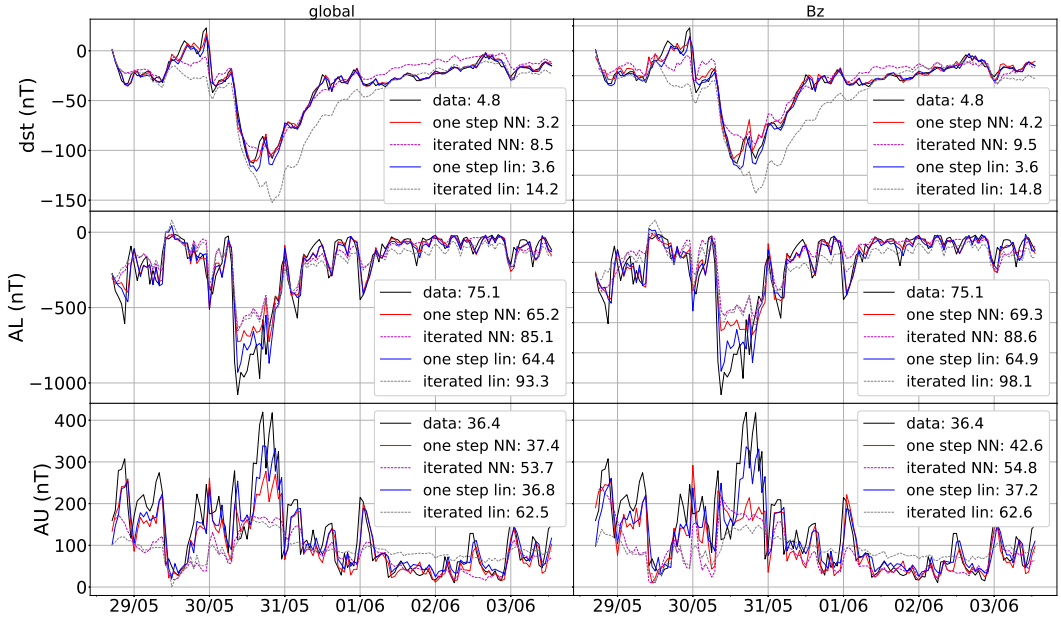

Figure 7. Forecasts of the geomagnetic indices during the storm of May 2005 for the (Left) Globally robust models and (Right) the B_z based models. The solid black line shows the data with a legend of MAE. Solid red (blue) corresponds to the one step prediction of NN (linear models).

Figure 7 shows the one step and iterated globally robust model forecasting during the storm of May 2013 that reached a Dst minimum of $-113\,\mathrm{nT}$. In the left panel we show the predictions for the globally robust NN and linear models and in the right panel we have results corresponding to the B_z-based models. The given numbers in the legend correspond to the bare MAE without normalization, and the errors of the different models (and one step vs. iterated) normalized to the persistence. The one step predictions show improvements from the B_z based model, for example Dst one step forecasting is improved by 23.8% when comparing the NN models. When looking at the iterated prediction, the globally robust model improves the Dst iterated prediction by 10.5% in this particular case. On the other hand, we highlight the notorious improvement for this storm of the error in Dst for the globally robust model of 40.1% between linear and NN models.

4 Conclusions

We have studied the correlation between geomagnetic indices (Dst, AU and AL) and interplanetary solar wind variables at the L1 point of the Sun-Earth system through 64 geomagnetic storms, for which we have simultaneous data, that occurred since 1995. The method we used is based on training Neural Networks and look at their capability to predict the evolution of the magnetosphere in storm periods. We stressed the entries of the trained Neural Networks in order to evaluate their robustness of the solar wind variables, at particular time delays, in the prediction of the geomagnetic indices. The magnetic z-component of the interplanetary magnetic field and the duskward oriented component of the electric field VB_z appeared to be the most robust drivers for the prediction since the addition of a noise to them shown a significant degradation in their capacity to drive the geomagnetic indices. By a similar method we determined which of the 9 solar wind variables, and particular time delays, we must consider in this analy-

sis to give the best predictions of the geomagnetic indices. We obtain that the relevance of the geomagnetic variables gets reduced considerably for $t \leq 3$ hours from the last measurement.

The pressure, the ϵ_A parameter, the temperature, the x and y components of the magnetic field, and the particle density of the interplanetary medium do not seem to bring significant contribution to the prediction at this level of approximation.

Finally we built a linear and nonlinear models based on the robust solar wind variables in their capability to forecast. We show that over a sample of 20 storms, the forecasting of Dst is improved by 12.7% from a Neural Network based only on the interplanetary z-component of the magnetic field that consider 11 time delays. Neural network are 38% better to predict Dst than linear models which emphasizes the highly non-linear behavior of the magnetosphere. Hence, the robust model, with only its 6 solar wind drivers, provides an improvement in the forecast of this simplified SWMI system representation. Of course, we could consider including robust magnetospheric indices at various time delays, as variables for the NN, a work that we plan to conduct in a future publication.

Future forecasting models of MIs should strongly consider the highlighted variables and time delays as input of their models. This is in particular true for Dst forecasting which is widely used to describe the state of the magnetosphere. Of course, additional information is provided about AL and AU, which are in general hard to obtain in real time. A similar method can be used to highlight the driving variables of other geomagnetic indices, like K_p or A_p, used in web services in order to improve the reliability of the forecasts. Those results can be used to construct step-by-step a multivariate, robust system science, description of the magnetosphere evolution.

Moreover, variables that show significant contribution at several time delays can be interpreted as orders in differential equation that can drive the MIs. Therefore it could improve existing minimal system-science mathematical descriptions of the magnetosphere behavior at the one hour time-scale.

It is worth noticing that the MI coupled model can be further used to test hypothesis of cross-predictability among the MIs, by using measured sequences of a subset of them to forecast, in an iterated scheme, the others by suing the measured MIs as input in the robust model proposed. Such analysis may help further our understanding of the so called "storm-substorm" coupling. This will be presented shortly.

Finally, these type of techniques can be used to find the relevant drivers in other nonlinear systems, where including too many variables in the NNs may be dangerous if we intend to produce robust forecasts. We plan to introduce other magnetospheric indices in a larger version of the SWMI system representation.

Acknowledgments

We acknowledge fruitful discussion with Joe Borovsky. We kindly thank the World Data Center for Geomagnetism, to provide openly data of the Dst geomagnetic index used in this study. We also acknowledge N. Papitashvili and J.King at the National Space Science Data Center of the Goddard Space Flight Center for the use permission of 1 min OMNI data and the NASA CDAWeb team for making these data available. We thank the support of Fondecyt Grant No. 1190703, US ASFOR Award No. FA9550-18-1-0438, and US ASFOR Award No. FA9550-19-1-0384.

References

Abiodun, O. I., Jantan, A., Omolara, A. E., Dada, K. V., Mohamed, N. A., & Arshad, H. (2018). State-of-the-art in artificial neural network applica-

tions: A survey. *Heliyon*, *4*(11), e00938. doi: https://doi.org/10.1016/j.heliyon.2018.e00938

Adhikari, B., Sapkota, N., Dahal, S., Bhattarai, B., Khanal, K., & Chapagain, N. (2020, 06). Spectral characteristic of geomagnetically induced current during geomagnetic storms by wavelet techniques.

Bala, R., & Reiff, P. (2018). Chapter 2 - data availability and forecast products for space weather. In E. Camporeale, S. Wing, & J. R. Johnson (Eds.), *Machine learning techniques for space weather* (p. 27 - 41). Elsevier. Retrieved from `http://www.sciencedirect.com/science/article/pii/B9780128117880000020` doi: https://doi.org/10.1016/B978-0-12-811788-0.00002-0

Bargatze, L. F., Baker, D. N., L., M. R., & Hones, E. W. (1985). Magnetospheric response to the imf: substorms. *Journal of Geophysical Research: Space Physics*, *90*, 6387.

Borovsky, J. E. (2020). A survey of geomagnetic and plasma time lags in the solar-wind-driven magnetosphere of earth. *Journal of Atmospheric and Solar-Terrestrial Physics*, *208*, 105376. Retrieved from `http://www.sciencedirect.com/science/article/pii/S1364682620301875` doi: https://doi.org/10.1016/j.jastp.2020.105376

Borovsky, J. E., & Denton, M. H. (2018). Exploration of a composite index to describe magnetospheric activity: Reduction of the magnetospheric state vector to a single scalar. *Journal of Geophysical Research: Space Physics*, *123*(9), 7384-7412. doi: 10.1029/2018JA025430

Borovsky, J. E., & Shprits, Y. Y. (2017). Is the dst index sufficient to define all geospace storms? *Journal of Geophysical Research: Space Physics*, *122*(11), 11,543-11,547. doi: 10.1002/2017JA024679

Borovsky, J. E., & Valdivia, J. A. (2018). The earth's magnetosphere: A systems science overview and assessment. *Surveys of Geophysics*, *39*(11), 817. doi: 10.1007/s10712-018-9487-x

Bortnik, J., Chu, X., Ma, Q., Li, W., Zhang, X., Thorne, R. M., ... Baker, D. N. (2018). Chapter 11 - artificial neural networks for determining magnetospheric conditions. In E. Camporeale, S. Wing, & J. R. Johnson (Eds.), *Machine learning techniques for space weather* (p. 279 - 300). Elsevier. Retrieved from `http://www.sciencedirect.com/science/article/pii/B9780128117880000111` doi: https://doi.org/10.1016/B978-0-12-811788-0.00011-1

Burton, R. K., McPherron, R. L., & Russell, C. T. (1975). An empirical relationship between interplanetary conditions and dst. *Journal of Geophysical Research: Space Physics*, *80*, 4204.

Camporeale, E. (2019). The challenge of machine learning in space weather: Nowcasting and forecasting. *Space Weather*, *17*(8), 1166-1207. Retrieved from `https://agupubs.onlinelibrary.wiley.com/doi/abs/10.1029/2018SW002061` doi: 10.1029/2018SW002061

Consolini, G., Alberti, T., & De Michelis, P. (2018). On the forecast horizon of magnetospheric dynamics: A scale-to-scale approach. *Journal of Geophysical Research: Space Physics*, *123*(11), 9065-9077. doi: 10.1029/2018JA025952

Council, N. R. (2008). *Severe space weather events: Understanding societal and economic impacts: A workshop report*. Washington, DC: The National Academies Press. Retrieved from `https://www.nap.edu/catalog/12507/severe-space-weather-events-understanding-societal-and-economic-impacts-a` doi: 10.17226/12507

Davis, T. N., & Sugiura, M. (1966). Auroral electrojet activity index ae and its universal time variations. *Journal of Geophysical Research (1896-1977)*, *71*(3), 785-801. doi: 10.1029/JZ071i003p00785

Donner, R. V., Balasis, G., Stolbova, V., Georgiou, M., Wiedermann, M., & Kurths,

J. (2019). Recurrence-based quantification of dynamical complexity in the earth's magnetosphere at geospace storm timescales. *Journal of Geophysical Research: Space Physics*, *124*(1), 90-108. doi: 10.1029/2018JA025318

Gosling, J. T. (2000). The solar flare myth. *Journal of Geophysical Research: Space Physics*, *98*, 18937.

Gruet, M. A., Chandorkar, M., Sicard, A., & Camporeale, E. (2018). Multiplehour-ahead forecast of the dst index using a combination of long short-term memory neural network and gaussian process. *Space Weather*, *16*, 1882-1896. doi: 10.1029/2018SW001898

Hapgood, M. (2018). Chapter 1 - societal and economic importance of space weather. In E. Camporeale, S. Wing, & J. R. Johnson (Eds.), *Machine learning techniques for space weather* (p. 3 - 26). Elsevier. Retrieved from `http://www.sciencedirect.com/science/article/pii/B9780128117880000019` doi: https://doi.org/10.1016/B978-0-12-811788-0.00001-9

Jawad, M., Rafique, A., Khosa, I., Ghous, I., Akhtar, J., & Ali, S. M. (2019, Feb). Improving disturbance storm time index prediction using linear and nonlinear parametric models: A comprehensive analysis. *IEEE Transactions on Plasma Science*, *47*(2), 1429-1444. doi: 10.1109/TPS.2018.2887202

King, J. H., & Papitashvili, N. E. (2005). Solar wind spatial scales in and comparisons of hourly wind and ace plasma and magnetic field data. *Journal of Geophysical Research: Space Physics*, *110*(A2). Retrieved from `https://agupubs.onlinelibrary.wiley.com/doi/abs/10.1029/2004JA010649` doi: 10.1029/2004JA010649

Lazzus, J. A., Vega, P., Rojas, P., & Salfate, I. (2017). Forecasting the dst index using a swarm-optimized neural network. *Space Weather*, *15*(8), 1068-1089. doi: 10.1002/2017SW001608

Masahito, N., Sugiura Masahisa, Kamei Toyohisa, Iyemori Toshihiko, & Yukinobu, K. (2015). *Dst index.* WDC for Geomagnetism, Kyoto. Retrieved from `http://isds-datadoi.nict.go.jp/wds/10.17593_14515-74000.html` doi: 10.17593/14515-74000

Sugiura, M. (1964, 1). Hourly values of equatorial dst for the igy. *Ann. Int. Geophys. Yr.*, *35*.

Valdivia, J., Rogan, J., Munoz, V., Toledo, B. A., & Stepanova, M. (2013). The magnetosphere as a complex system. *Advances of Space Research*, *51*, 1934.

Valdivia, J. A., Rogan, J., Munoz, V., Gomberoff, L., Klimas, A. J., Vassiliadis, D., ... Wastavino, B. T. L. (2005). The magnetosphere as a complex system. *Advances of Space Research*, *35*, 961-971.

Valdivia, J. A., Sharma, A. S., & Papadopoulos, K. (1996). Prediction of magnetic storms by nonlinear models. *Geophysical Research Letters*, *23*(21), 2899-2902. doi: 10.1029/96GL02828

Valdivia, J. A., Vassiliadis, D., & Klimas, A. J. (1999). Modeling the spatial structure of the high latitude magnetic perturbation in the related current system. *Physics of Plasmas*, *6*, 4185-4194.

Vassiliadis, D., Klimas, A. J., Baker, D. N., & Roberts, D. A. (1995). A description of the solar wind-magnetosphere coupling based on nonlinear filters. *Journal of Geophysical Research: Space Physics*, *100*, 3495-3512.

Vassiliadis, D., Klimas, A. J., Valdivia, J. A., & Baker, D. N. (1999). The dst geomagnetic response as a function of storm phase and amplitude and the solar wind electric field. *Journal of Geophysical Research: Space Physics*, *104*, 24957.

Vassiliadis, D., Klimas, A. J., Valdivia, J. A., & Baker, D. N. (2000). The nonlinear dynamics of space weather. *Advances of Space Research*, *26*, 197.

data_set_repartition.

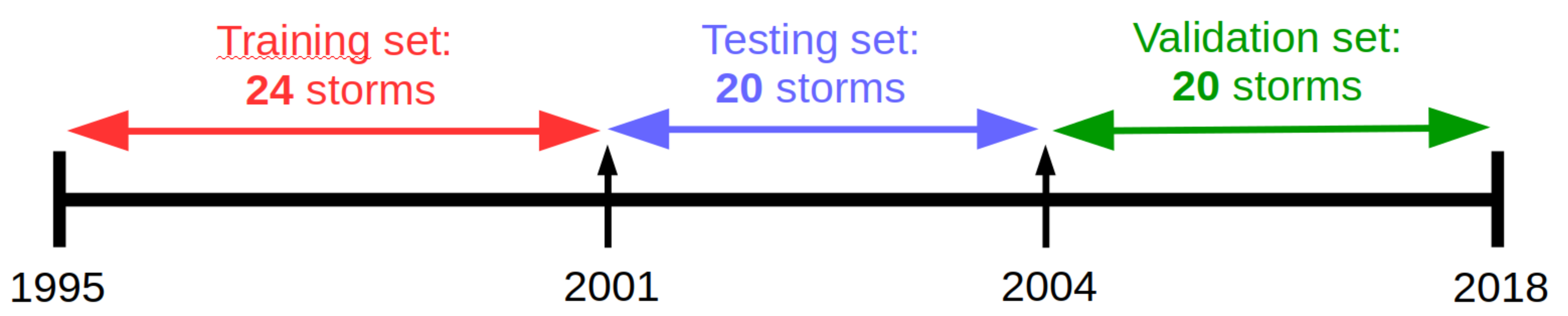
Training set:
24 storms
Testing set:
20 storms
Validation set:
20 storms
1995
2001
2004
2018

NN_representation.

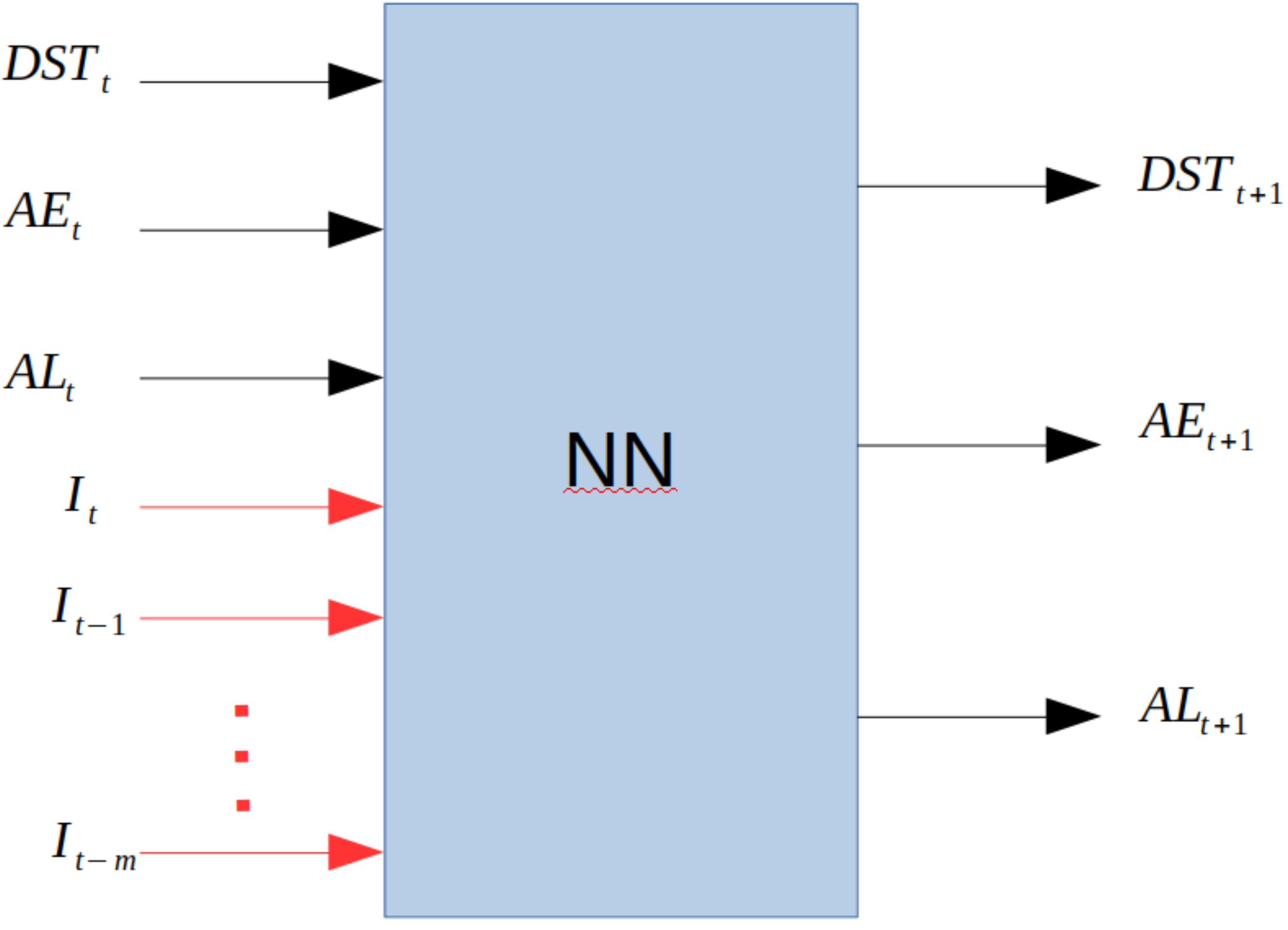
DST_t
AE_t
AL_t
I_t
I_{t-1}
I_{t-m}
NN
DST_{t+1}
AE_{t+1}
AL_{t+1}

sigma.

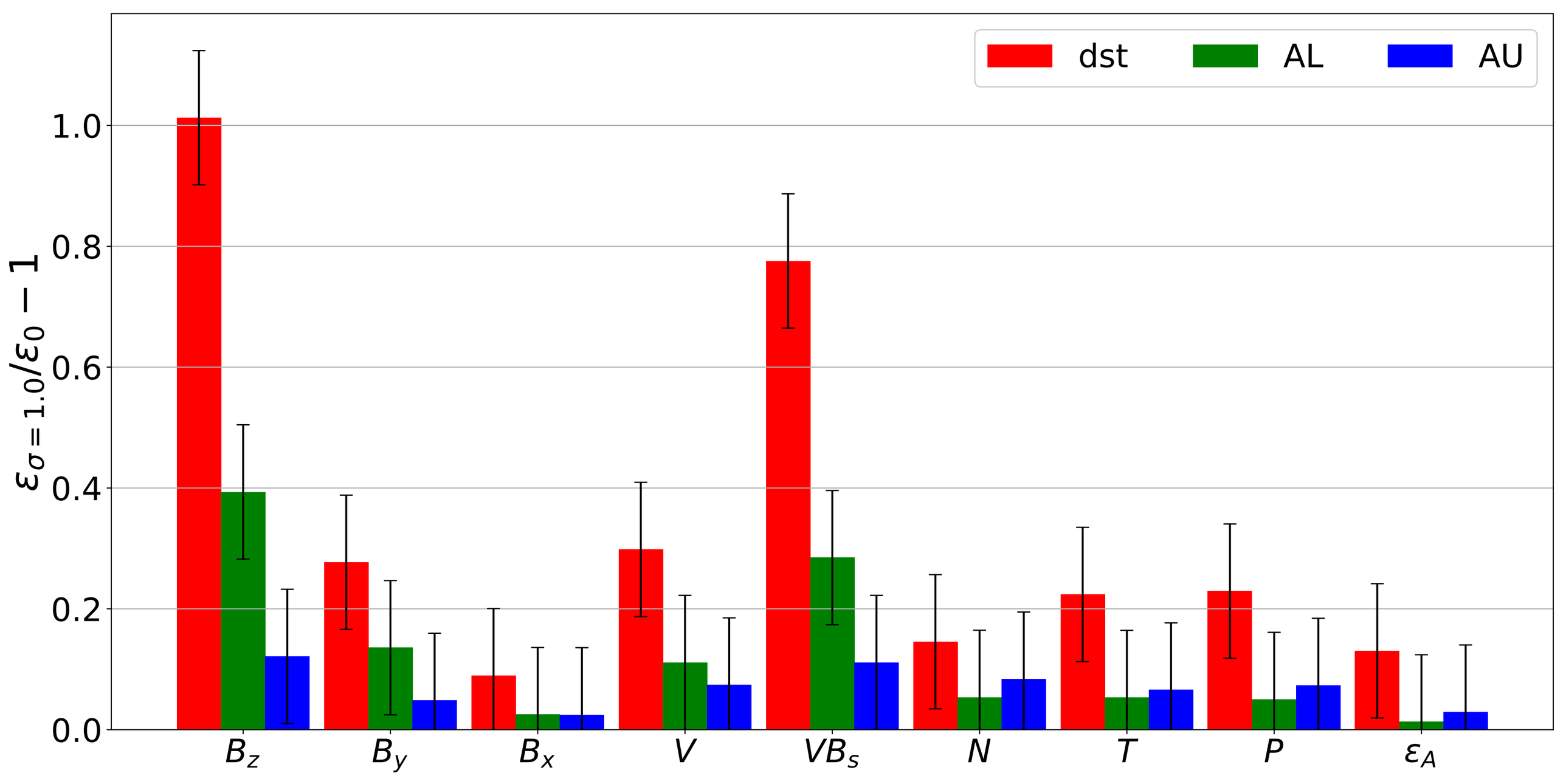
dst
AL
AU
$\varepsilon_{\sigma=1.0}/\varepsilon_0 - 1$
0.0
0.2
0.4
0.6
0.8
1.0
B_z
B_y
B_x
V
VB_s
N
T
P
ε_A

AU_tau.

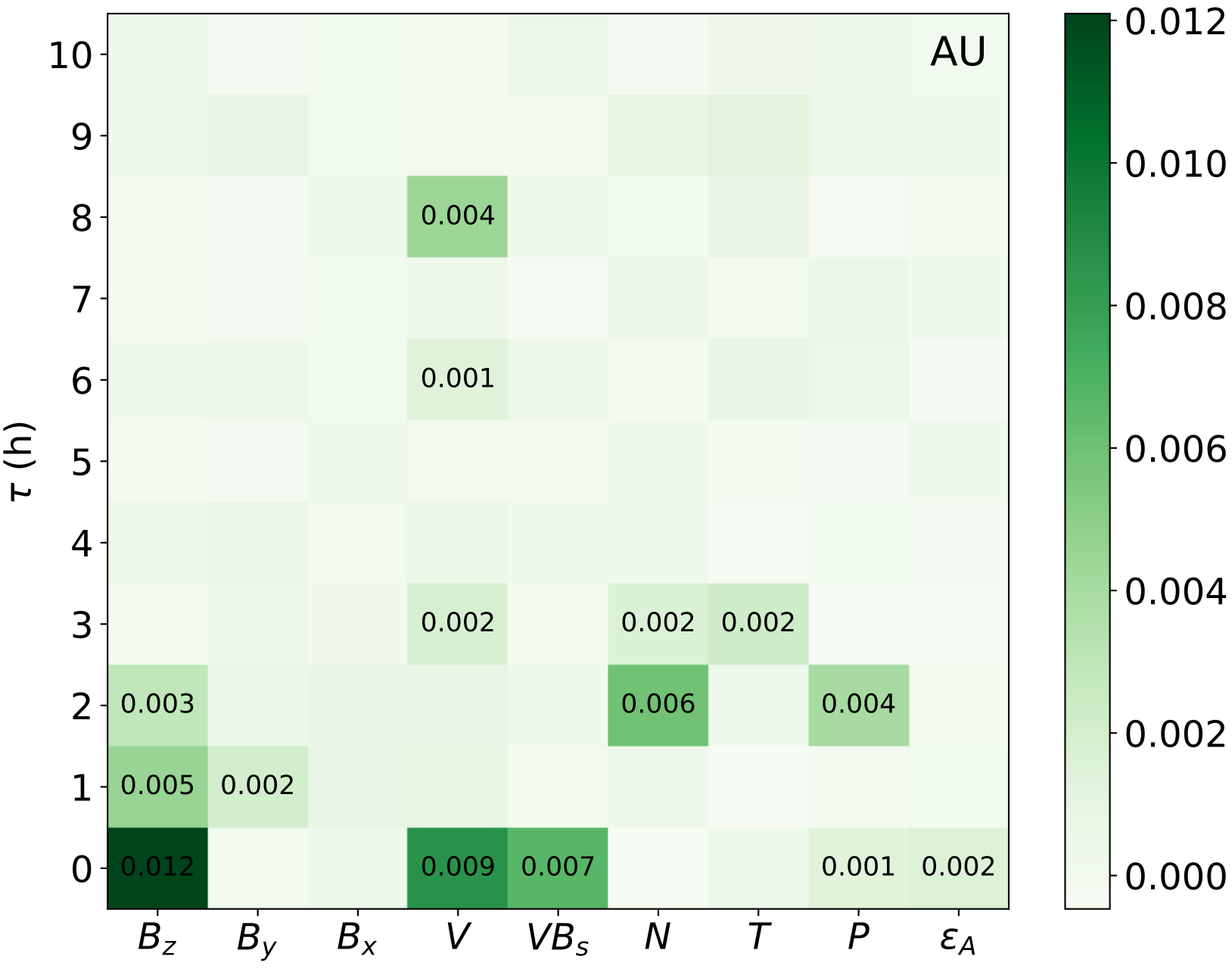
AU
τ (h)
10
9
8
7
6
5
4
3
2
1
0
0.004
0.001
0.002
0.002
0.003
0.006
0.004
0.005
0.002
0.012
0.009
0.007
0.001
0.002
B_z
B_y
B_x
V
VB_s
N
T
P
ε_A
0.012
0.010
0.008
0.006
0.004
0.002
0.000

dst_tau.

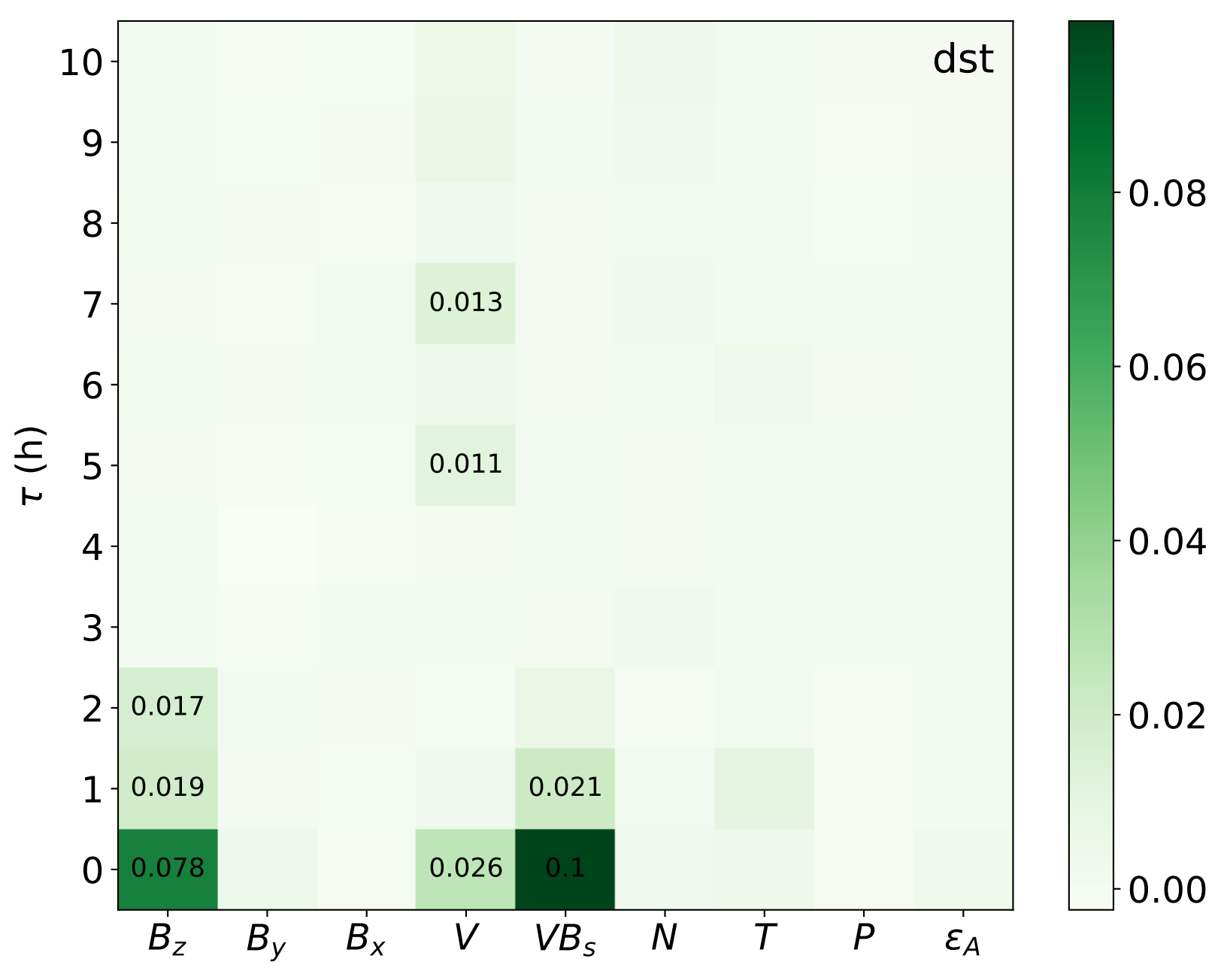
dst
τ (h)
10
9
8
7
6
5
4
3
2
1
0
0.013
0.011
0.017
0.019
0.021
0.078
0.026
0.1
B_z
B_y
B_x
V
VB_s
N
T
P
ε_A
0.08
0.06
0.04
0.02
0.00

AL_tau.

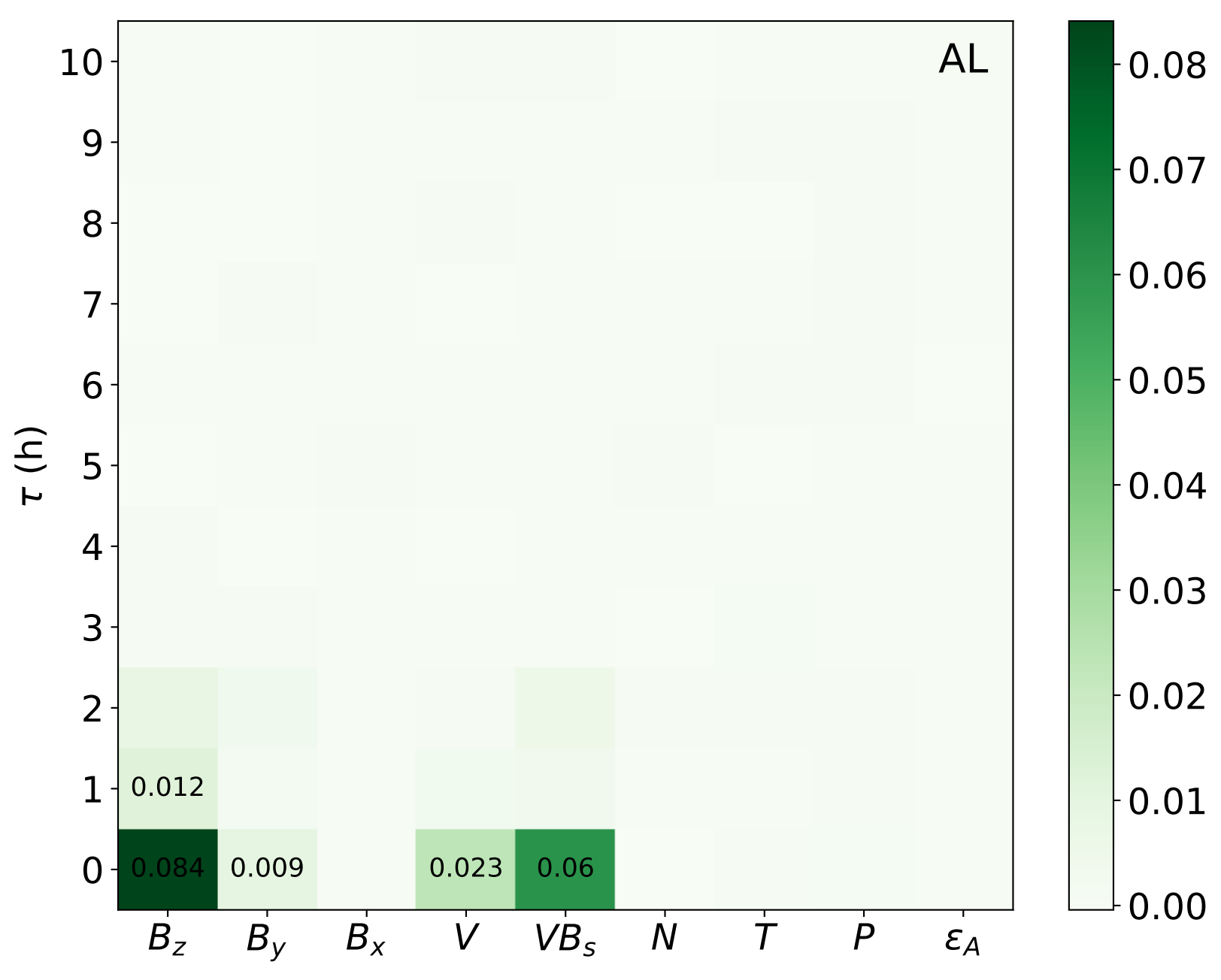
AL
τ (h)
10
9
8
7
6
5
4
3
2
1
0
0.012
0.084
0.009
0.023
0.06
B_z
B_y
B_x
V
VB_s
N
T
P
ε_A
0.08
0.07
0.06
0.05
0.04
0.03
0.02
0.01
0.00

sum_histog.

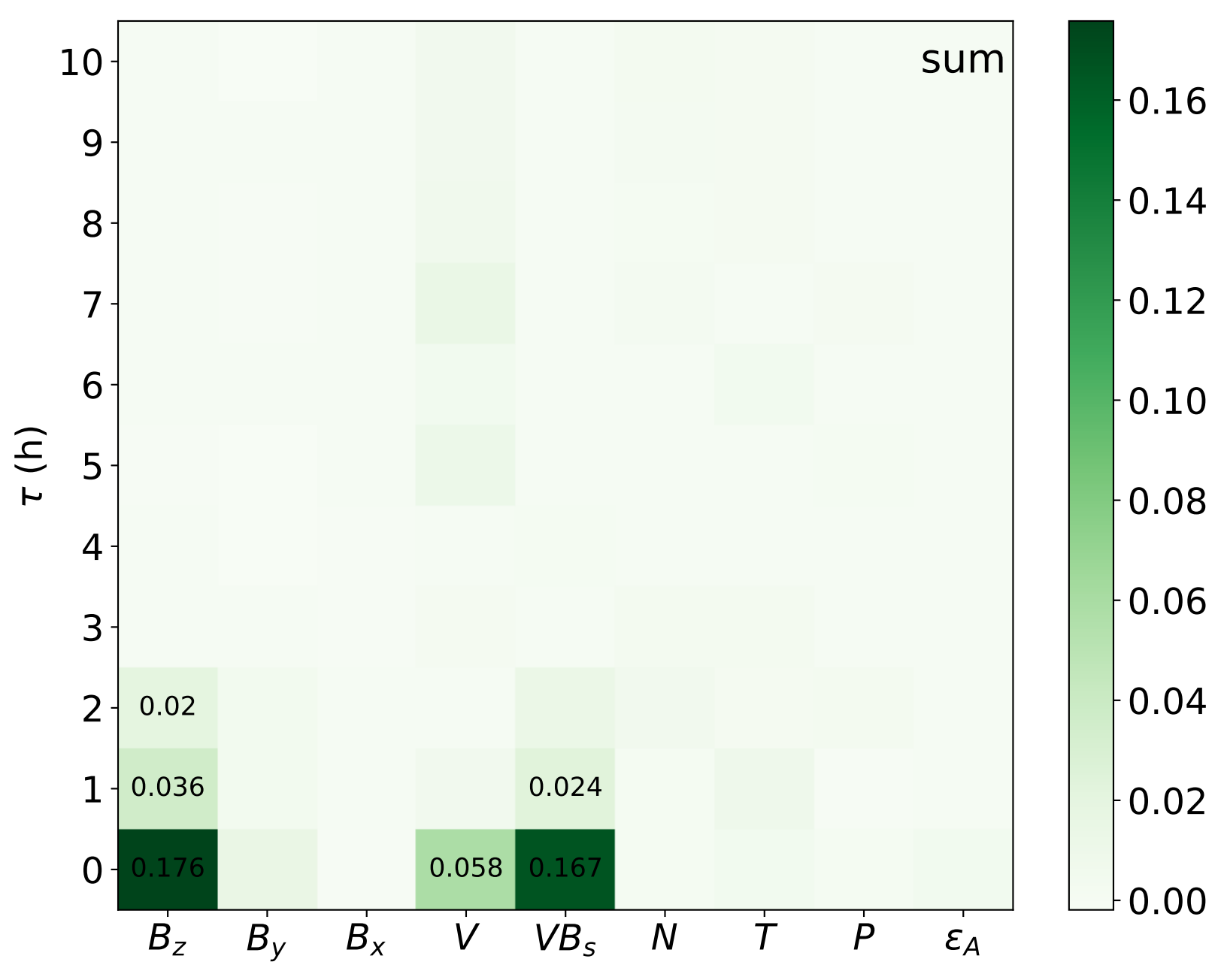
sum
τ (h)
10
9
8
7
6
5
4
3
2
1
0
0.02
0.036
0.024
0.176
0.058
0.167
B_z
B_y
B_x
V
VB_s
N
T
P
ε_A
0.16
0.14
0.12
0.10
0.08
0.06
0.04
0.02
0.00

global_validation_histog_ND.

Input: $(B_z^{t-0}, B_z^{t-1}, B_z^{t-2}, V^{t-0}, VB_s^{t-0}, VB_s^{t-1})$ + GIs

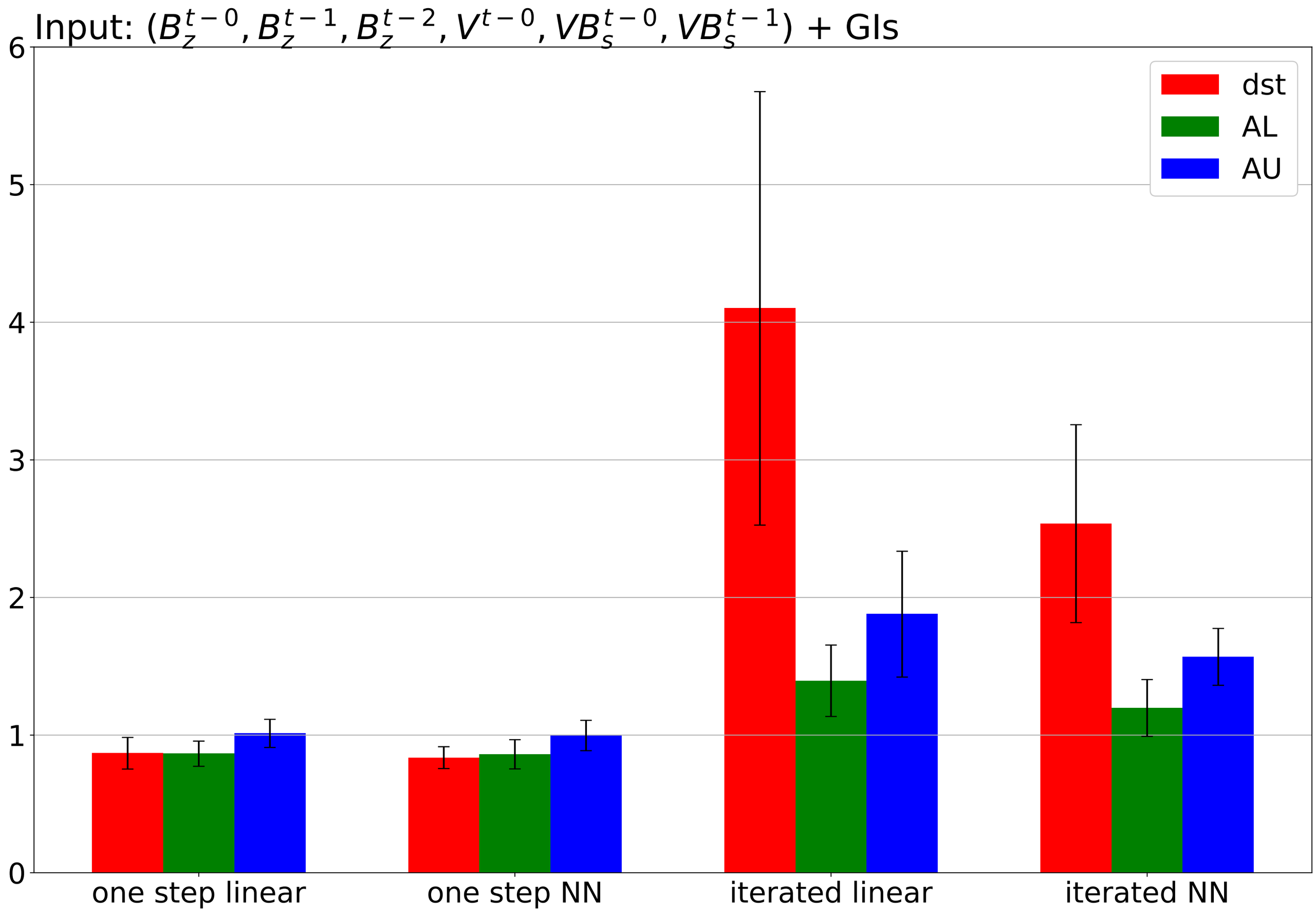

20050530.

global

Bz

dst (nT)

0
−50
−100
−150

data: 4.8
one step NN: 3.2
iterated NN: 8.5
one step lin: 3.6
iterated lin: 14.2

data: 4.8
one step NN: 4.2
iterated NN: 9.5
one step lin: 3.6
iterated lin: 14.8

AL (nT)

0
−500
−1000

data: 75.1
one step NN: 65.2
iterated NN: 85.1
one step lin: 64.4
iterated lin: 93.3

data: 75.1
one step NN: 69.3
iterated NN: 88.6
one step lin: 64.9
iterated lin: 98.1

AU (nT)

400
300
200
100
0

data: 36.4
one step NN: 37.4
iterated NN: 53.7
one step lin: 36.8
iterated lin: 62.5

data: 36.4
one step NN: 42.6
iterated NN: 54.8
one step lin: 37.2
iterated lin: 62.6

29/05
30/05
31/05
01/06
02/06
03/06

29/05
30/05
31/05
01/06
02/06
03/06

Bz_validation_histog.

Input: 11 B_z entries + GIs

dst
AL
AU

0
1
2
3
4
5
6

one step linear
one step NN
iterated linear
iterated NN

onestep_20010320.

dst

AL

AU

vbs
pressure
By
temperature
Bx
Bz
ε_A
speed
density

σ (%)